Extended Range of Dipole-Dipole Interactions in Periodically Structured Photonic Media

Lei Ying,[1] Ming Zhou,[1] Michael Mattei,[2] Boyuan Liu,[1] Paul Campagnola,[3]
Randall H. Goldsmith,[2] and Zongfu Yu[1,*]
[1]Department of Electrical and Computer Engineering, University of Wisconsin, Madison, Wisconsin 53706, USA
[2]Department of Chemistry, University of Wisconsin, Madison, Wisconsin 53706, USA
[3]Department of Biomedical Engineering, University of Wisconsin, Madison, Wisconsin 53706, USA

(Received 27 May 2019; published 23 October 2019)

The interaction between quantum two-level systems is typically short range in free space and in most photonic environments. We show that diminishing momentum isosurfaces with equal frequencies can create a significantly extended range of interaction between distant quantum systems. The extended range is robust and does not rely on a specific location or orientation of the transition dipoles. A general relation between the interaction range and properties of the isosurface is described for structured photonic media. It provides a new way to mediate long-range quantum behavior.

DOI: 10.1103/PhysRevLett.123.173901

The resonant dipole-dipole interaction between two quantum two-level systems (TLSs) is typically short range. There has been strong interest in realizing long-range interactions to exploit collective physics such as superradiance [1,2], collective frequency shift [3], Förster resonance energy transfer [4,5], and quantum entanglement [6–12]. The ability to modulate the distance dependence of these processes could have potential applications in quantum information processing [8,13] and energy conversion [14]. Two components contribute to the interaction: the evanescent near fields and the propagating far fields [Figs. 1(a) and 1(b)]. To enable long-range interaction from the evanescent fields, one could use evanescent fields with a long tail, such as defect modes in the photonic band gap [15–17]. However, it is less obvious how to engineer propagating far fields to enable long-range interaction. It is the goal of this Letter to provide a new perspective to understand the general physical mechanism that is responsible for long-range interaction induced by propagating far fields, and to identify photonic structures that are capable of extending the interaction range.

In free space, the range of far-field interaction is limited to the wavelength scale. When the wavelength is long, such as in index-near-zero materials [18–22], the interaction range can increase proportionally. However, there are a few intriguing examples where the interaction range extends beyond the effective wavelength. These include low-dimensional spaces, such as photonic crystal waveguides and fibers [2,23–30], or hyperbolic materials in selected directions [31,32]. These interesting but isolated examples rely heavily on very specific configurations. Thus, it is difficult to generalize the theoretical treatments to identify the underlying physics, which unfortunately remains elusive. In this Letter, we show the deep connection between the interaction range and the size and shape of the isofrequency surface in momentum space. It can be generalized to a broad range of physical systems and can reveal new systems capable of realizing long-range interactions.

We begin by examining the interaction between two TLSs over a long distance. The TLSs are embedded in a photonic environment that can be described by a dispersion relation $\omega = \omega(\mathbf{k})$. For example, in free space, $\omega = c|\mathbf{k}| = ck$, where c is the speed of light. Other dispersion relations can be seen in metamaterials, photonic crystals, or waveguides. In general, the Hamiltonian of the TLSs and the photonic modes is given by [33]

$$\mathcal{H} = \sum_{i=1,2} \omega_0 \hat{\sigma}_i^\dagger \hat{\sigma}_i + \sum_{\mathbf{k}} \omega_{\mathbf{k}} \hat{a}_{\mathbf{k}}^\dagger \hat{a}_{\mathbf{k}} + i \sum_{i=1,2} \sum_{\mathbf{k}} [i g_{\mathbf{k}}(\mathbf{r}_i)(\hat{\sigma}_i^\dagger - \hat{\sigma}_i)\hat{a}_{\mathbf{k}}^\dagger e^{-i\mathbf{k}\cdot\mathbf{r}_i} + H.c.], \quad (1)$$

where ω_0 is the resonant transition frequency of the TLSs. $\hat{\sigma}_i^\dagger(\hat{\sigma}_i)$ is the raising (lowering) operator of the ith TLS.

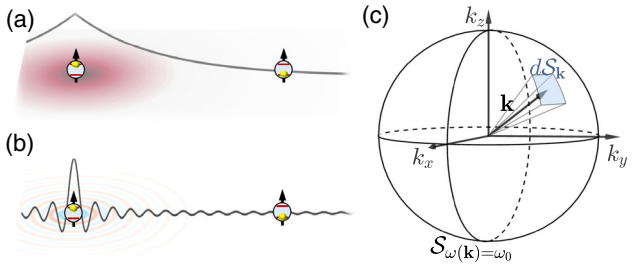

FIG. 1. Schematics of interactions between two TLSs mediated by (a) evanescent near-field modes and (b) propagating far-field modes. (c) The momentum isosurface $S_{\omega(\mathbf{k})=\omega_0}$ with equal frequencies ω_0 and $dS_{\mathbf{k}}$ is a small surface element.

$\omega_{\mathbf{k}}$ and $\hat{a}^{\dagger}_{\mathbf{k}}(\hat{a}_{\mathbf{k}})$ are the frequency and creation (annihilation) operator of the photons, respectively. $g_{\mathbf{k}}(\mathbf{r}_i) = \sqrt{\omega_k/2\varepsilon_0 V}\boldsymbol{\mu}_i \cdot \boldsymbol{\epsilon}_{\mathbf{k}}$ is the coupling between the ith TLS and the photonic mode $\mathbf{k}$, where $\boldsymbol{\mu}_i$ is the transition dipole moment of the ith TLS and $\boldsymbol{\epsilon}_{\mathbf{k}}$ is the polarization direction of the photonic mode $\mathbf{k}$. One can derive the radiative interaction $\Gamma = \Gamma_{\mathrm{Re}} + i\Gamma_{\mathrm{Im}}$ between two TLSs based on the above Hamiltonian. The real and imaginary parts describe the cooperative decay rate and the cooperative energy shift, respectively. The focus of this Letter will be the cooperative decay rate. Similar conclusions can be drawn for the cooperative energy shift.

We first provide a graphic illustration of why the interaction between TLSs is short range in free space. Unlike most theoretical treatments used in the literature [32], we do not use the Green's function method to describe the radiative environment. Instead, we try to keep all radiative modes in their explicit forms in order to gain a more intuitive picture. As shown in Sec. I of the Supplemental Material (SM) [34], the real part of the radiative interaction between the TLSs can be expressed in the following form:

$$\Gamma_{\mathrm{Re}} = \iint_{S_{\omega_0(\mathbf{k})}} \rho_{\mathbf{k}} e^{i\mathbf{k}\cdot\mathbf{R}} dS_{\mathbf{k}}. \tag{2}$$

The integration is performed on an isosurface in momentum space, i.e., all wave vectors $\mathbf{k}$ that satisfy $\omega(\mathbf{k}) = \omega_0$. The integrand includes two terms. The first term is simply a polarization factor $\rho_{\mathbf{k}} = [\omega_0/16\varepsilon_0\pi^2 v_g(\mathbf{k})](\boldsymbol{\mu}_1 \cdot \boldsymbol{\epsilon}_{\mathbf{k}})(\boldsymbol{\mu}_2 \cdot \boldsymbol{\epsilon}_{\mathbf{k}})^*$, which describes the relative orientation of the transition dipole $\boldsymbol{\mu}$ and the polarization of the electric field $\boldsymbol{\epsilon}$. Here $v_g(\mathbf{k})$ is the group velocity of mode $\mathbf{k}$. For degenerate polarization states, the integration should also include all polarizations. Since the polarization factor $\rho_{\mathbf{k}}$ is independent of the inter-TLS distance, it does not affect the interaction range. It is the second term, $e^{i\mathbf{k}\cdot\mathbf{R}}$, that plays the critical role in the physics of the interaction range. Here $\mathbf{R} = \mathbf{r}_2 - \mathbf{r}_1$ is the distance vector between the two TLSs. The integrand $\rho_{\mathbf{k}} e^{i\mathbf{k}\cdot\mathbf{R}}$ is a fast-oscillating function, which generally results in cancellation of the integration when the inter-TLS distance R is large. Therefore, the interaction is always short range. We can see this effect in Fig. 2(a). Here we consider two TLSs in free space. The spherical isosurface has a radius of $k = |\mathbf{k}| = \omega_0/c$. The real part of $\rho_k e^{i\mathbf{k}\cdot\mathbf{R}}$ is plotted on the isosurface. When $R = 10\lambda$, there are rapid oscillations as $\mathbf{k}$ varies on the isosurface. The resulting value of the integral is small, and therefore the interaction is weak at this long distance. When the inter-TLS distance is small, for example $R = 0.3\lambda$, the oscillation is slow [Fig. 2(c)], leading to a sizable value of the integral and thus a strong interaction. The interaction decays as the distance R grows [Fig. 2(d)].

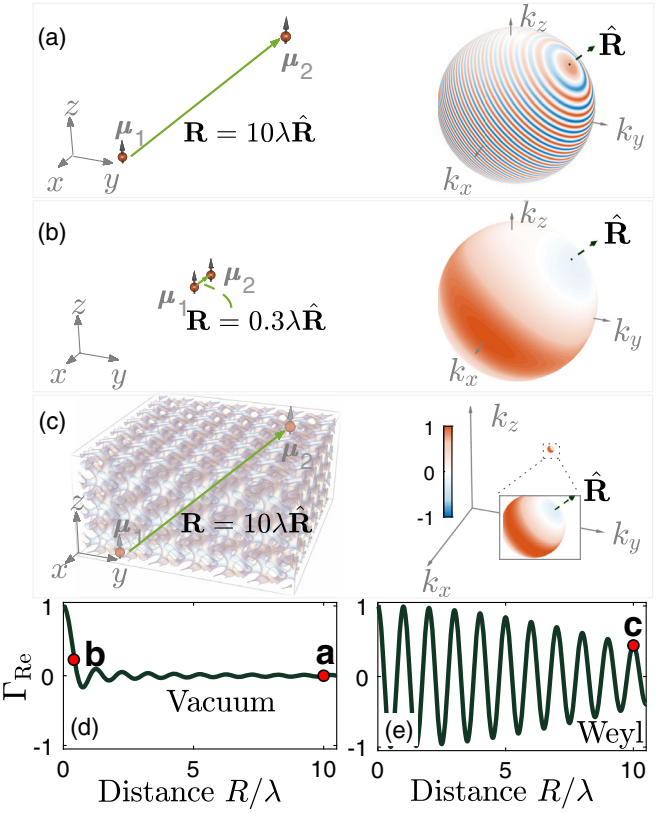

FIG. 2. (a) Two dipolar TLSs spaced by a distance $R = 10\lambda$ in free space, where $\lambda = 2\pi c/\omega$. (Right panel) Isosurface for the transition frequency in momentum space. The real part of $\rho_{\mathbf{k}} e^{i\mathbf{k}\cdot\mathbf{R}}$ is plotted on the isosurface. Red and blue colors indicate positive and negative maxima, respectively. (b) Similar to (a) but with a shorter distance $R = 0.3\lambda$ and thus slow oscillation on the isosurface. (c) Two TLSs are placed in a specific photonic environment, such as a Weyl photonic crystal, where the isosurface radius, $q = |\mathbf{k} - \mathbf{k}_c|$, can be very small. Here $R = 10\lambda$. $\hat{\mathbf{R}}$ in (a)–(c) is fixed as $(1, 0, 1)/\sqrt{2}$. (d),(e) The real part of radiative interaction, normalized by $\Gamma_{\mathrm{Re}}(R = 0)$, as a function of distance between two TLSs in free space and the Weyl photonic crystal, respectively. Red dots correspond to the cases in (a)–(c), respectively.

The graphic illustration also indicates that the interaction range is *inversely* proportional to the size of the isosurface in momentum space. A large inter-TLS distance R on a large isosurface leads to a fast-oscillating integrand on the isosurface that results in a small value of the integral. One way to counteract this effect is to substantially reduce the isosurface size. Small isosurfaces can save the integral from cancellation even for a fast-oscillating function. Figure 2(c) shows the real part of the integrand $\rho_{\mathbf{k}} e^{i\mathbf{k}\cdot\mathbf{R}}$ with a long inter-TLS distance $R = 10\lambda$ on an isosurface that has a radius that is 0.03 times that of the free-space isosurface. While the oscillation is still fast, the small isosurface cannot accommodate many oscillations, yielding a sizable value of the integral. Figure 2(e) shows that this strong interaction is sustained over a long distance if the isosurface is small. Specifically, for an isosurface with a radius of q, the real

part of interaction Γ_{Re} scales as $\sin(qR)/qR$. As the isosurface radius approaches zero, $q \to 0$, the range becomes infinite. Here we use a polarization factor $\rho_{\mathbf{k}}$ based on plane waves which, although a simplification, is sufficient for estimating the scaling.

The size of isosurface is fixed in free space. But there are many structured photonic environments that offer smaller isosurfaces. Here we use Weyl photonic crystals as an example to demonstrate the inverse relationship between the interaction range and the isosurface. Weyl photonic crystals [36,38] exhibit a conic dispersion relation in 3D space, similar to Dirac dispersion relations in 2D space. The isosurface gradually reduces to a point around the apex of the conic dispersion, i.e., the Weyl point. Observation of this small isosurface suggests that we could expect long-range interactions around isolated Weyl points. Specifically, we consider a double-gyroid structure with four air spherical defects [Fig. 3(a)] to break parity symmetry, yielding two pairs of Weyl points at identical frequencies [39]. The dispersion relation on the plane of $k_z = 0$ is shown in Fig. 3(b) with two pairs of Weyl points at the frequency $\omega_{\mathrm{wp}} = 0.550\,96[2\pi c/a]$. The isosurface becomes infinitesimally small at the Weyl point.

Using these isosurfaces, we numerically calculate the interaction between two TLSs placed inside the Weyl crystal. The photonic modes are simulated using the MPB software package [37]. The details of the calculation are shown in the SM [34]. Figure 3(c) shows the interaction as a function of the inter-TLS distance for three different transition frequencies, which are also labeled by white lines in Fig. 3(b). The isosurfaces have four lobes because there are four Weyl points, as shown in Figs. 3(c)(i)–3(c)(iii). As the TLS transition frequency approaches the Weyl point, the isosurface size decreases, causing the interaction to extend to a significantly greater range. When the transition frequency is $0.000\,24[2\pi c/a]$ away from the Weyl point [Fig. 3(c)(iii)], the interaction shows a negligible decay even at 180 wavelengths [Fig. 3(c), bottom panel].

The decaying and oscillating patterns in these curves are attributed to a few different origins. At the largest scale, the envelope scales as $\sin(\bar{q}R)/\bar{q}R$, where we use $\bar{q}$ to roughly characterize the size of the subsurface (we will discuss the impact of the shape of the isosurface later). The medium-range oscillation is due to the interplay of four Weyl points at the same frequency. The fastest oscillation is due to the modulation of the nonuniform field within a unit cell of the photonic crystal. The long-range interaction observed here is robust in that it does not rely on the orientation of the dipole direction or the spatial placement of the TLSs (see the SM for more discussion [34]).

We can quantitatively characterize the interaction range by numerically fitting the envelope. These envelopes are shown with the dashed line in Fig. 3(c). We further define a range ℓ_D as the distance when the envelope drops to half of its maximum value. We calculate this range for TLSs at different transition frequencies near the Weyl points, corresponding to different isosurface sizes. The results are shown in Fig. 3(d). A clear linear relationship is demonstrated between ℓ_D and the inverse of the isosurface size $1/\bar{q}$. Because the isosurfaces are not spherical, we use $\bar{q} = \sqrt{S_\omega/4\pi}$ to define the isosurface size, where S_ω is the surface area of the isosurfaces.

Thus far, we have shown that the size of the isosurface plays a critical role in the interaction range. Next, we will

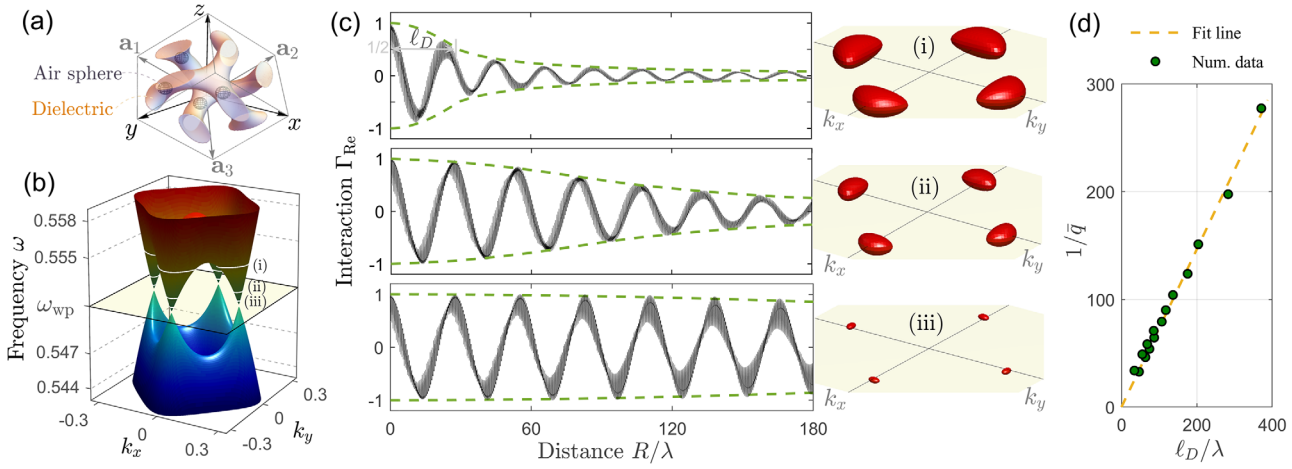

FIG. 3. (a) Structure of the Weyl photonic crystal. A double-gyroid dielectric unit cell with four air spherical defects is the same as in Ref. [39]. (b) Dispersion relation on the plane of $k_z = 0$. $k_{x,y}$ are normalized by $2\pi/a$, where a is the lattice constant. (c) The real part of the radiative interaction Γ_{Re} [normalized by $\Gamma_{\mathrm{Re}}(R=0)$] as a function of distance for TLS transition frequencies (upper panel) $\omega = 0.5545$, (middle panel) 0.5520, and (lower panel) $0.5512[2\pi c/a]$, which are marked with white contours (i), (ii), and (iii) in (b), respectively. The inter-TLS direction is $\hat{\mathbf{R}} = (-1,1,1)/\sqrt{3}$. The dipole orientations are $\hat{\boldsymbol{\mu}}_{1,2} = (-1,1,1)/\sqrt{3}$, and $\boldsymbol{\mu}_1$ is fixed at a central point of the unit cell. Green dashed curves are the envelopes of the solid curves. Insets (i)–(iii) are the isosurfaces in momentum space. (d) The linear relationship between the decay length ℓ_D "and the inverse of the isosurface size $1/\bar{q}$.

discuss the role of the shape of the isosurface. A spherical isosurface leads to an isotropic interaction range. On the other hand, a nonspherical isosurface generally creates an anisotropic interaction range: the interaction range depends on the direction of the inter-TLS distance vector $\hat{\mathbf{R}}$. There is a general reciprocal relationship between the interaction range and the size of the isosurface when projected along $\hat{\mathbf{R}}$.

Let us take the example of an ellipsoidal isosurface in an anisotropic medium. The interaction range is longer when the two TLSs are placed along the direction of the short axis of the ellipsoid $\hat{\boldsymbol{s}}$ than when they are along the long axis $\hat{\boldsymbol{l}}$. We can easily see this effect by observing the oscillation pattern of $\rho_{\mathbf{k}} e^{i\mathbf{k}\cdot\mathbf{R}}$ on an ellipsoidal isosurface as shown in Fig. 4(a). When $\hat{\mathbf{R}}$ is parallel to the long axis $\hat{\boldsymbol{l}}$, we have many oscillations and strong cancellation of the integration. On the other hand, when $\hat{\mathbf{R}}$ is parallel to the short axis $\hat{\boldsymbol{s}}$, we have fewer oscillations and weaker cancellation.

To demonstrate this effect in Weyl photonic crystals, we plot the isosurface at frequency $\omega = \omega_{\mathrm{wp}} + 0.00404[2\pi c/a]$, where the isosurface has a flat edge-softened rectangular geometry [Fig. 4(b)]. We plot the real part of the integrand in Eq. (2) on the isosurface for three different $\mathbf{R}$. Here the magnitude of $\mathbf{R}$ is fixed, but its direction $\hat{\mathbf{R}}$ varies from the short axis $\hat{\boldsymbol{s}}$ to the long axis $\hat{\boldsymbol{l}}$. The cancellation effect is weaker when $\mathbf{R}$ is aligned with the short axis and stronger along the long axis. We also calculate the interaction as a function of the distance for the three directions shown in Fig. 4(b). The range is conspicuously longer for TLSs placed along the short axis of the isosurface than along the long axis, as shown in Fig. 4(c). In the case shown in Fig. 4, the frequency is greatly detuned from the Weyl point, and thus the interaction range is not as long as those shown in Fig. 3.

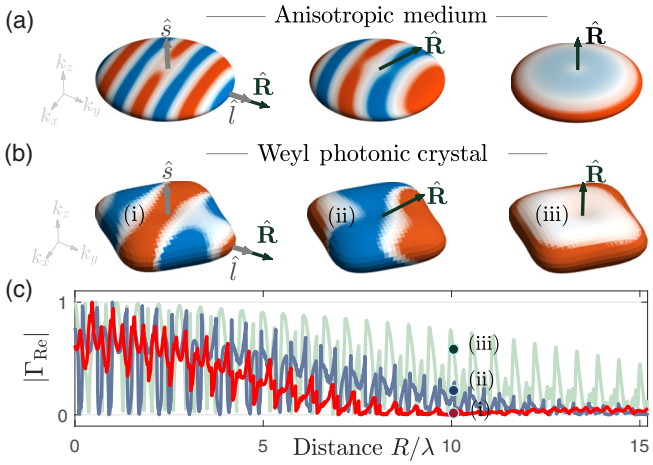

FIG. 4. (a) Real part of the integrand in Eq. (2) on an elliptical isosurface with (left panel) $\hat{\mathbf{R}} = (0, 1, 0)$, (middle panel) $\hat{\mathbf{R}} = (0, 1, 1)/\sqrt{2}$, and (right panel) $\hat{\mathbf{R}} = (0, 0, 1)$. Unit vectors $\hat{\boldsymbol{s}}$ and $\hat{\boldsymbol{l}}$ represent the short and long axes of the anisotropic isosurface. The dipole orientation is fixed as $\hat{\boldsymbol{\mu}}_{1,2} = (0, 0, 1)$. (b) The same as (a), except that the isosurface is in the Weyl photonic crystal in Fig. 3(a) at frequency $\omega = 0.555[2\pi c/a]$ and the dipole orientation is fixed at $\hat{\boldsymbol{\mu}}_{1,2} = (0, 1, 0)$. (c) The absolute value of Γ_{Re} as a function of distance R. Light green, blue, and red curves, respectively, correspond to $\hat{\mathbf{R}}$ in the left, middle, and right cases of (b).

The extended range of the dipole-dipole interaction extends beyond quantum systems. In the microwave regime, where Weyl photonic crystals have been experimentally realized on a printed circuit board [38], the resonant dipole-dipole interaction range can also be extended. The range will also be limited by the propagation length of the waves inside such systems due to finite absorption by the metallic materials.

We also emphasize that the relation between the interaction range and the isosurface is not unique to Weyl photonic crystals. It is generally applicable to periodically structured media. For example, in 2D space, the scaling of the interaction range follows $J_0(kR)$, where J_0 is the Bessel function of the first kind. For a 2D photonic crystal, a spherical isosurface with a radius of q creates a different scaling law that follows $J_0(qR)$. More examples are discussed in Sec. II of the SM [34].

We have discussed the interaction range. Another important aspect is the strength of the interaction. We choose the linear dispersion near the Weyl points because it makes it easy to separate the effect of the isosurface from other effects such as group velocity and density of states. However, the shrinking isosurface combined with a finite group velocity also decreases the interaction strength. At the Weyl point, the interaction strength is zero. The linear dispersion near a Weyl point results in a trade-off between the interaction range and strength. Such a trade-off can be alleviated in 2D crystals and with a high order dispersion relation. We discuss the scaling of the interaction strength in Sec. II in the SM [34].

Visual inspection of the isosurface provides a convenient tool for understanding a broad class of long-range interaction phenomena. We now comment on the connection between our approach and the existing literature. The behavior of index-near-zero materials [18] was explained by a long effective wavelength. Alternatively, it can also be conveniently explained by our method: the index-near-zero material also has an ultrasmall isosurface. In addition to these examples, we can envision that Dirac points in 2D photonic crystals also provide small "isosurfaces" (isofrequency contours) for a long-range interaction. Reference [16] shows that *inside* the photonic band gap, long tails of evanescent fields can induce a long-range interaction. Here we can also see that *outside* the photonic band gap but near the band edge, the propagating far fields have small isosurfaces, offering a different mechanism for long-range interaction. A hyperbolic material, where long-range interactions were allowed along specific directions, was treated using the Green's function method [32].

Using our graphic interpretation allows one to intuitively see that only special directions allow long-range interactions (see the visualization in the SM [34]).

To conclude, we show in this Letter the deep connection between the interaction range and the isosurface in momentum space. Both the size and the shape of the isosurface affect the interaction range. The method introduced here provides an intuitive understanding of underlying physics that is somewhat buried in traditional treatments, and we are able to use our method to help us understand several photonic systems in the existing literature. Our method also provides a general recipe to search for new photonic systems that support long-range interactions.

This work was supported by the National Science Foundation (NSF) through the University of Wisconsin Materials Research Science and Engineering Center DMR-1720415. L. Y. and Z. Y. were also supported by the Defense Advanced Research Projects Agency (DARPA) (DETECT program). L. Y. also acknowledges financial support from NSF EFRI Grant No. 1641109.

*zyu54@wisc.edu

[1] M. O. Scully and A. A. Svidzinsky, Science **325**, 1510 (2009).
[2] P. Solano, P. Barberis-Blostein, F. K. Fatemi, L. A. Orozco, and S. L. Rolston, Nat. Commun. **8**, 1857 (2017).
[3] Z. Meir, O. Schwartz, E. Shahmoon, D. Oron, and R. Ozeri, Phys. Rev. Lett. **113**, 193002 (2014).
[4] R. M. Clegg, Curr. Opin. Biotechnol. **6**, 103 (1995).
[5] F. J. Garcia-Vidal and J. Feist, Science **357**, 1357 (2017).
[6] A. F. Van Loo, A. Fedorov, K. Lalumière, B. C. Sanders, A. Blais, and A. Wallraff, Science **342**, 1494 (2013).
[7] G. Burkard and A. Imamoglu, Phys. Rev. B **74**, 041307(R) (2006).
[8] D. Petrosyan and M. Fleischhauer, Phys. Rev. Lett. **100**, 170501 (2008).
[9] S. F. Mingaleev, Y. S. Kivshar, and R. A. Sammut, Phys. Rev. E **62**, 5777 (2000).
[10] A. Gonzalez-Tudela, D. Martin-Cano, E. Moreno, L. Martin-Moreno, C. Tejedor, and F. J. Garcia-Vidal, Phys. Rev. Lett. **106**, 020501 (2011).
[11] E. Shahmoon and G. Kurizki, Phys. Rev. A **87**, 033831 (2013).
[12] J. D. Hood, A. Goban, A. Asenjo-Garcia, M. Lu, S.-P. Yu, D. E. Chang, and H. Kimble, Proc. Natl. Acad. Sci. U.S.A. **113**, 10507 (2016).
[13] A. Imamoglu, D. D. Awschalom, G. Burkard, D. P. DiVincenzo, D. Loss, M. Sherwin, A. Small, Phys. Rev. Lett. **83**, 4204 (1999).
[14] D. Maxwell, D. J. Szwer, D. Paredes-Barato, H. Busche, J. D. Pritchard, A. Gauguet, K. J. Weatherill, M. P. A. Jones, and C. S. Adams, Phys. Rev. Lett. **110**, 103001 (2013).
[15] G. Kurizki, Phys. Rev. A **42**, 2915 (1990).
[16] J. S. Douglas, H. Habibian, C.-L. Hung, A. V. Gorshkov, H. J. Kimble, and D. E. Chang, Nat. Photonics **9**, 326 (2015).
[17] V. Notararigo, R. Passante, and L. Rizzuto, Sci. Rep. **8**, 5193 (2018).
[18] R. Fleury and A. Alù, Phys. Rev. B **87**, 201101(R) (2013).
[19] A. Mahmoud, I. Liberal, and N. Engheta, Opt. Mater. Express **7**, 415 (2017).
[20] I. Liberal and N. Engheta, Phys. Rev. A **97**, 022309 (2018).
[21] F. T. Gundogdu, A. E. Serebryannikov, A. O. Cakmak, and E. Ozbay, Opt. Express **23**, 24120 (2015).
[22] A. E. Serebryannikov, H. Hajian, M. Krawczyk, G. A. Vandenbosch, and E. Ozbay, Opt. Mater. Express **9**, 3169 (2019).
[23] Y. Sato, Y. Tanaka, J. Upham, Y. Takahashi, T. Asano, and S. Noda, Nat. Photonics **6**, 56 (2012).
[24] F. Le Kien and A. Rauschenbeutel, Phys. Rev. A **95**, 023838 (2017).
[25] G. Lecamp, P. Lalanne, and J. P. Hugonin, Phys. Rev. Lett. **99**, 023902 (2007).
[26] S. Hughes, Phys. Rev. Lett. **98**, 083603 (2007).
[27] P. Yao and S. Hughes, Opt. Express **17**, 11505 (2009).
[28] M. Minkov and V. Savona, Phys. Rev. B **87**, 125306 (2013).
[29] C. Hung, S. Meenehan, D. Chang, O. Painter, and H. Kimble, New J. Phys. **15**, 083026 (2013).
[30] J. P. Vasco, P. S. S. Guimaraes, and D. Gerace, Phys. Rev. B **90**, 155436 (2014).
[31] S.-A. Biehs, V. M. Menon, and G. S. Agarwal, Phys. Rev. B **93**, 245439 (2016).
[32] C. L. Cortes and Z. Jacob, Nat. Commun. **8**, 14144 (2017).
[33] S. Bay, P. Lambropoulos, and K. Mølmer, Phys. Rev. A **55**, 1485 (1997).
[34] See Supplemental Material at http://link.aps.org/supplemental/10.1103/PhysRevLett.123.173901, which includes Refs. [15,32,33,35–37], for more derivation details and discussions in different photonic environments.
[35] D. L. Andrews and D. S. Bradshaw, Eur. J. Phys. **25**, 845 (2004).
[36] L. Lu, L. Fu, J. D. Joannopoulos, and M. Soljačić, Nat. Photonics **7**, 294 (2013).
[37] S. G. Johnson and J. D. Joannopoulos, Opt. Express **8**, 173 (2001).
[38] B. Yang, Q. Guo, B. Tremain, R. Liu, L. E. Barr, Q. Yan, W. Gao, H. Liu, Y. Xiang, J. Chen *et al.*, Science **359**, 1013 (2018).
[39] L. Wang, S.-K. Jian, and H. Yao, Phys. Rev. A **93**, 061801(R) (2016).